

Maximum A Posteriori Ly- α Estimator (MAPLE): Band-power and covariance estimation of the 3D Ly- α forest power spectrum

Benjamin Horowitz,^{1,2*} Roger de Belsunce,^{2,3} Zarija Lukić²

¹Kavli IPMU (WPI), UTIAS, The University of Tokyo, Kashiwa, Chiba 277-8583, Japan

²Lawrence Berkeley National Laboratory, One Cyclotron Road, Berkeley CA 94720, USA

³Berkeley Center for Cosmological Physics, Department of Physics, University of California, Berkeley, CA 94720, USA

Accepted XXX. Received YYY; in original form ZZZ

ABSTRACT

We present a novel maximum a posteriori estimator to jointly estimate band-powers and the covariance of the three-dimensional power spectrum (P3D) of Ly- α forest flux fluctuations, called MAPLE. Our Wiener-filter based algorithm reconstructs a window-deconvolved P3D in the presence of complex survey geometries typical for Ly- α surveys that are sparsely sampled transverse to and densely sampled along the line-of-sight. We demonstrate our method on idealized Gaussian random fields with two selection functions: (i) a sparse sampling of 30 background sources per square degree designed to emulate the currently observing the Dark Energy Spectroscopic Instrument (DESI); (ii) a dense sampling of 900 background sources per square degree emulating the upcoming Prime Focus Spectrograph Galaxy Evolution Survey. Our proof-of-principle shows promise, especially since the algorithm can be extended to marginalize jointly over nuisance parameters and contaminants, i.e. offsets introduced by continuum fitting. Our code is implemented in JAX and is publicly available on GitHub.

Key words: methods: statistical, numerical – Cosmology: large-scale structure of Universe, theory – galaxies: statistics

1 INTRODUCTION

Clustering statistics of large-scale structure tracers carry a wealth of information about dark energy and dark matter. For cosmological inference, the observed data vector is usually compressed to a summary statistic specific to the observed tracer. For the Ly- α forest flux fluctuations, a series of absorption features in quasar and galaxy spectra due to intervening neutral hydrogen in the highly ionized intergalactic medium (IGM) along the line of sight (Scheuer 1965; Gunn & Peterson 1965), two main approaches have been used for cosmological data analysis:

First, the dense sampling along the line-of-sight motivated measuring the one-dimensional, or line-of-sight, Ly- α power spectrum (Croft et al. 1999, 2002; Kim et al. 2004; McDonald et al. 2005; Palanque-Delabrouille et al. 2013; Chabanier et al. 2019; Pedersen et al. 2021; Karacayli et al. 2022; Ravoux et al. 2023). It is a unique probe which puts tight constraints on dark matter models from the small scale clustering (Viel et al. 2013; Villasenor et al. 2023; Iršič et al. 2024), non-minimal cosmological models (Garny et al. 2018; Goldstein et al. 2023), exotic physics models (i.e. Viel et al. (2013); Iršič et al. (2017)) and, on larger scales, constrains the Λ CDM model (Palanque-Delabrouille et al. 2013; Yèche et al. 2017).

Second, the sparse sampling of the Ly- α forest transverse to the line-of-sight leads to adoption of the two-point correlation function (2PCF) to measure the baryonic acoustic oscillation (BAO) feature to constrain the expansion history of our Universe (Sunyaev & Zel'dovich 1970; Peebles & Yu 1970; Seo & Eisenstein 2003; Slosar et al. 2011, 2013a; McDonald & Eisenstein 2007; Slosar et al. 2013b;

Busca et al. 2013; du Mas des Bourboux et al. 2020) and the broadband shape of 3D correlations (Slosar et al. 2013b; Cuceu et al. 2021, 2023; Gordon et al. 2023). The Ly- α forest is a treasure trove of cosmological information on the large-scale distribution of matter in the Universe and probes the underlying matter density at Mpc scales and below at high redshifts ($2 \lesssim z \lesssim 5$).

A pioneering study on the P3D from realistic simulations (Font-Ribera et al. 2018) and recent measurements of the 3D Ly- α power spectrum (Karim et al. 2023; de Belsunce et al. 2024) together with advancements in the theoretical modeling of the Ly- α forest power spectrum (see e.g., Ivanov 2023, and references therein), have sparked interest in the three-dimensional power-spectrum containing information across lines of sight – a case in point for our work. Whilst both summary statistics, the 2PCF and P3D, contain, in principle, the same information, both have their advantages (Font-Ribera et al. 2018): The power spectrum isolates slowly varying features at large scales while having (potentially) less correlated errors. The 2PCF can be calculated using simple pixel-product algorithms and can isolate effects at specific separations, like the BAO peak. Whilst the 2PCF can easily deal with the window matrix, grid-based FFT estimators for the P3D are strongly affected by the sparse sampling of the Ly- α forest (de Belsunce et al. 2024).

In this paper, we present the Maximum A Posteriori Ly- α Estimator, MAPLE, which can efficiently estimate the 3D Ly- α power spectrum in band-powers with a corresponding covariance matrix from idealized Gaussian random fields (GRF) with non-trivial survey geometries and varying number densities, typical for Ly- α forest surveys. To test the accuracy of the band-power reconstruction, we

* E-mail: bahorowitz@lbl.gov

emulate two background source density configurations¹: (i) the Dark Energy Spectroscopic Instrument (DESI, [DESI Collaboration et al. \(2016\)](#)) with ~ 30 background sources per deg^2 ; and (ii) the Prime Focus Spectrograph (PFS, [Greene et al. \(2022\)](#)) with ~ 900 background sources per deg^2 .

Our estimator expands on earlier work for power spectrum and covariance estimation in more general contexts ([Seljak et al. 2017](#); [Horowitz et al. 2019b](#)), which we extend to the three-dimensional case for the present work. We utilize a modern implementation of a response-type formalism, known as the Marginal Unbiased Score Estimator (MUSE) ([Millea & Seljak 2022](#); [Millea 2022](#)), to estimate the band-powers and associated covariance matrices. We implement our code in JAX, which enables modern implicit differentiable models and optimization methods for rapid estimation even in high dimensional spaces, and supports graphical processor unit (GPU) architecture. We make our implementation publicly available.²

The remainder of this paper is organized as follows: We present the 3D power spectrum estimator in Sec. 2, before discussing the theoretical modeling of the Ly- α flux power spectrum in Sec. 3. In Sec. 4 we describe our idealized Gaussian random fields and compare the reconstructed band-powers to the theory input power spectrum in Sec. 5. In Sec. 6 presents our conclusions.

2 METHODS

We present a novel approach to compress the Ly- α forest flux fluctuations to the 3D power spectrum using a minimization-based approach. We briefly outline the methodology and focus on Ly- α -specific implementation details and refer the reader to [Seljak et al. \(2017\)](#); [Horowitz et al. \(2019b\)](#) for a fuller presentation.

2.1 Marginal Unbiased Score Estimation

We want to find the conditional probability distribution of our band-powers, θ , given some observed data, x , which we express as $\mathcal{P}(x|\theta)$. However, the data itself depends on N latent parameters, z . From those, in turn, some depend on the phases, θ , and others are nuisance parameters and, thus, do not depend on θ . This hierarchical Bayesian problem can be expressed as a marginalization over the latent space parameters,

$$\mathcal{P}(x|\theta) = \int d^N z \mathcal{P}(x, z|\theta) = \int d^N z \mathcal{P}(x|z, \theta) \mathcal{P}(z|\theta), \quad (1)$$

where $\mathcal{P}(x, z|\theta)$ is the joint likelihood of the data and the latent space parameters, given a fixed θ . In generic cases, this integral is analytically intractable and approximating it relies on Monte Carlo based sampling. More recently, methods have been developed to approximate this integral expression, including the Marginal Unbiased Score Estimation (MUSE) which is the focus of this work ([Seljak et al. 2017](#); [Horowitz et al. 2019b](#); [Millea & Seljak 2022](#)). The core idea of MUSE is to reformulate this integral as an optimization problem for $\mathcal{P}(x, z|\theta)$ for fixed θ and x , and iteratively solve for θ .

More concretely, at a fixed value of θ we want to find the maximum a posteriori value (MAP) for z defined by

$$\hat{z}(\theta, x) \equiv \underset{z}{\operatorname{argmax}} \log \mathcal{P}(x, z|\theta). \quad (2)$$

¹ Note that we focus on the effect of the window matrix and ignore contaminants such as the non-Gaussian resolution matrix, continuum fitting, metal contamination, damped Ly- α absorbers and broad absorption lines.

² <https://github.com/bhorowitz/MAPLE>

It can be shown that the derivatives of the likelihood function at the MAP estimate with respect to the parameters of interest, known as the ‘score’ are optimal statistics in the sense that they preserve all information content of the data ([Alsing & Wandelt 2018](#)). This score function can be expressed as

$$s_i^{\text{MAP}}(\theta, x) \equiv \frac{d}{d\theta_i} \log \mathcal{P}(x, \hat{z}(\theta, x) | \theta). \quad (3)$$

We define the MUSE estimate, $\bar{\theta}$ as the value of θ which satisfied the following equation

$$s_i^{\text{MAP}}(\theta, x) - \left\langle s_i^{\text{MAP}}(\theta, x) \right\rangle_{x \sim \mathcal{P}(x|\theta)} = 0, \quad (4)$$

where the second term is an ensemble average over realizations of the data drawn from $\mathcal{P}(x|\theta)$. This ensemble average can be viewed as a generalization of a noise bias which includes all possible sources of biasing from the forward model (i.e. survey geometry).

We can define the covariance matrix associated with this estimate as $\Sigma = H^{-1} J H^\dagger$, where J and H are defined as

$$J_{ij} = \left\langle s_i^{\text{MAP}}(\bar{\theta}, x) s_j^{\text{MAP}}(\bar{\theta}, x) \right\rangle_{x \sim \mathcal{P}(x|\bar{\theta})} - \left\langle s_i^{\text{MAP}}(\bar{\theta}, x) \right\rangle_{x \sim \mathcal{P}(x|\bar{\theta})} \left\langle s_j^{\text{MAP}}(\bar{\theta}, x) \right\rangle_{x \sim \mathcal{P}(x|\bar{\theta})}, \quad (5)$$

$$H_{ij} = \frac{d}{d\theta_j} \left[\left\langle s_i^{\text{MAP}}(\bar{\theta}, x) \right\rangle_{x \sim \mathcal{P}(x|\theta)} \right] \Big|_{\theta=\bar{\theta}}. \quad (6)$$

For a Gaussian likelihood, it can be shown that this definition provides directly the marginal maximum likelihood estimate and the covariance, Σ , becomes the inverse Fisher information matrix. Moreover, for a non-Gaussian likelihood, it has been shown that this definition provides an unbiased estimate, although the covariance may not be optimal ([Millea & Seljak 2022](#)). Note that we can also use this approach to generalize Fisher forecasts, wherein we do not perform the optimization discussed in Eq. (4) but instead assume a fixed value of the target quantity x .

We base our analysis code on the JAX implementation of MUSE³ discussed in [Millea & Seljak \(2022\)](#) using the implicit differentiation approach ([Millea 2022](#)) for the Hessian/Jacobian calculations in Eq. (5) and 6.

2.2 Cosmological Wiener Filtered Tomographic Reconstruction

A key step in the MUSE procedure described above is the inference of the latent space parameters, z for given observed data x . This requires a generative response model which may depend on fixed parameters, θ , i.e. R_θ . The generic optimal solution for this problem is the Wiener filter which, in the linear case, can be expressed in terms of the noise covariance N and signal covariance S , as

$$\hat{s} = S R_\theta^\dagger (S + N)^{-1} x. \quad (7)$$

In the case of the Ly- α forest (as well as many other large-scale structure probes), the signal covariance is assumed to be that of a fiducial cosmological model and the noise covariance is dominated by detector noise. The former is diagonal in Fourier space, while the latter is near diagonal in real space. Therefore, the resulting matrix inversion of $(S+N)$ is computationally demanding and often is recast

³ https://github.com/marius311/muse_inference

as an optimization problem (Seljak et al. 2017; Horowitz et al. 2019b) with associated χ^2 of

$$\chi^2(s_i) = s_i^\dagger S^{-1} s_i + (R_\theta s_i - d)^\dagger N^{-1} (R_\theta s_i - d), \quad (8)$$

where s_i is the guess at the i th optimization step.

This approach to Wiener Filtering is in contrast to the smooth priors used in many Ly- α tomography works (Caucci et al. 2008; Lee et al. 2018; Newman et al. 2020; Kraljic et al. 2022; Horowitz et al. 2022a). These methods are likely more optimal for cosmic web studies, where non-linear non-Gaussian structures are of interest, but smoothness priors are difficult to consistently interpret for cosmological analysis within a Bayesian framework.

We implement Eq. (8) as an optimization problem utilizing particle-mesh routines developed in Li et al. (2022). In our case, the latent space parameters z are the phases of the three-dimensional field, although we note it could be expanded to include nuisance parameters (e.g. continuum fitting parameters) which we leave to future work. The response function, R_θ , can be broken down into the following steps;

- (i) The phases, z , are convolved with a transfer function which is determined by the band-powers, θ .
- (ii) The resulting field is inverse Fourier transformed to real space.
- (iii) The values of the real space field are read out at the locations of mock observed data using a linear weighting scheme (i.e. Cloud-in-Cell readout (Laux 1995)) of nearby cells.

3 THEORY POWER SPECTRUM

To model the theory power spectrum, we employ the Kaiser formula (Kaiser 1987) with a non-linear correction term obtained from hydrodynamical simulations (see McDonald 2003; Arinyo-i-Prats et al. 2015). In order to perform our analysis we need to choose a basis/binning for our band-powers, θ . We emphasize that an advantage of our approach is that we apply the power spectrum as a transfer function on the full density field, meaning that this approach is agnostic to the chosen power spectrum basis. We define our power spectra in binned k_\perp , k_\parallel space with a constant redshift across the bin.

For our proof-of-concept, we focus on the usual redshift-space formula derived from the linear theory of gravitational collapse (Kaiser 1987) which includes effects obtained from fits to hydrodynamical simulations (McDonald 2003);

$$P_F(k, \mu) = b^2 (1 + \beta \mu^2)^2 P_L(k) D(k, \mu), \quad (9)$$

where $P_F(k, \mu)$ is the flux power spectrum as a function of wavevector k and angle $\mu \equiv k_\parallel/k$, b is the redshift-dependent linear bias parameter, β the redshift-space distortion (RSD) parameter, $P_L(k)$ the linear power spectrum⁴ and $D(k, \mu)$ a non-linear correction term:

$$D(k, \mu) = \exp \left(\left[\frac{k}{k_{\text{NL}}} \right]^{\alpha_{\text{NL}}} - \left[\frac{k}{k_{\text{P}}} \right]^{\alpha_{\text{P}}} - \left[\frac{k_\parallel}{k_{\text{V}}(k)} \right]^{\alpha_{\text{V}}} \right), \quad (10)$$

with

$$k_{\text{V}}(k) = k_{\text{V}0} \left(1 + \frac{k}{k'_{\text{V}}} \right)^{\alpha'_{\text{V}}}. \quad (11)$$

This formula accounts for effects from non-linear evolution

⁴ We compute it using the Boltzmann solver CAMB (<https://camb.info/>).

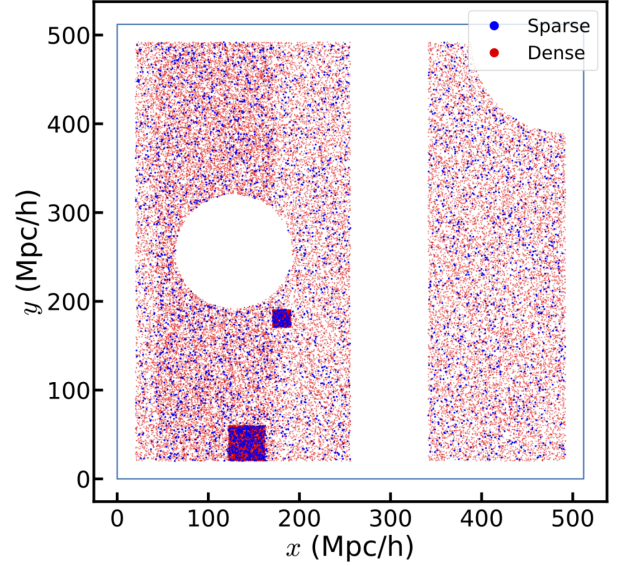


Figure 1. Mask used for the Gaussian random field for the dense (red) and sparse (blue) configurations, including irregularly masked areas and deep fields. We reconstruct an additional $10 h^{-1}$ Mpc on each edge to minimize boundary edge effects.

(NL), pressure smoothing (P), and velocity effects (V). We choose the values obtained from hydrodynamical simulations McDonald (2003) for $\{b^2, \beta, k_{\text{NL}}, \alpha_{\text{NL}}, k_{\text{P}}, \alpha_{\text{P}}, k_{\text{V}0}, \alpha_{\text{V}}, k'_{\text{V}}, \alpha'_{\text{V}}\} = \{0.0173, 1.58, 6.40, 0.569, 15.3, 2.01, 1.220, 1.50, 0.923, 0.451\}$. We set the cosmological parameters to be $\{\Omega_b, \Omega_m, h, A_s \times 10^9, n_s\} = \{0.02214, 0.1414, 0.719, 2.2, 0.961\}$.

4 GAUSSIAN RANDOM FIELD SIMULATIONS

We test MAPLE on an idealized Gaussian realization of our fiducial power spectrum on a $512 h^{-1}$ Mpc box, with resolution of 128^3 . This allows us to reconstruct up to $k_{\text{max}} = 0.81 h \text{ Mpc}^{-1}$.⁵ We use 11 bins, logarithmically spaced from $k_{\text{min}} = 0.001 h \text{ Mpc}^{-1}$ to k_{max} for both k_\perp and k_\parallel . The choice of bin number to use depends on the range of interest, noise properties of the observations, and the volume/resolution of the reconstructed volume. We choose this binning to allow identification of the large scale turnover and the small scale suppression of power. We perform our analysis at a constant fiducial redshift of $z = 2.0$.⁶

We use two survey configurations: (i) sparse which is inspired by the DESI number density of ~ 30 sources per deg^2 which roughly follows the noise/survey properties of Karaçaylı et al. (2020). We assume constant resolution power of $R = 3200$ and a constant signal-to-noise per angstrom of 2 (corresponding to $\sigma_F = 0.7$ per resolution element). (ii) The dense configuration is inspired by the Prime Focus Spectrograph Galaxy Evolution Survey (Greene et al. 2022), which targets both QSOs and Lyman Break Galaxies at greater depth ($g < 24.2$) although at a comparable spectral resolution as DESI. This broader targeting will allow a significantly greater number density of ~ 1000 background sources per deg^2 . For this larger and denser

⁵ The resolution for our MAP reconstruction is implicitly set by k_{max} .

⁶ In practice, each redshift bin would require a separate MUSE optimization. One could also restructure the procedure described in Sec 2.2 to treat sub-volumes relating to each redshift bin as having different band-power values (i.e. including a varying third dimension to the transfer function).

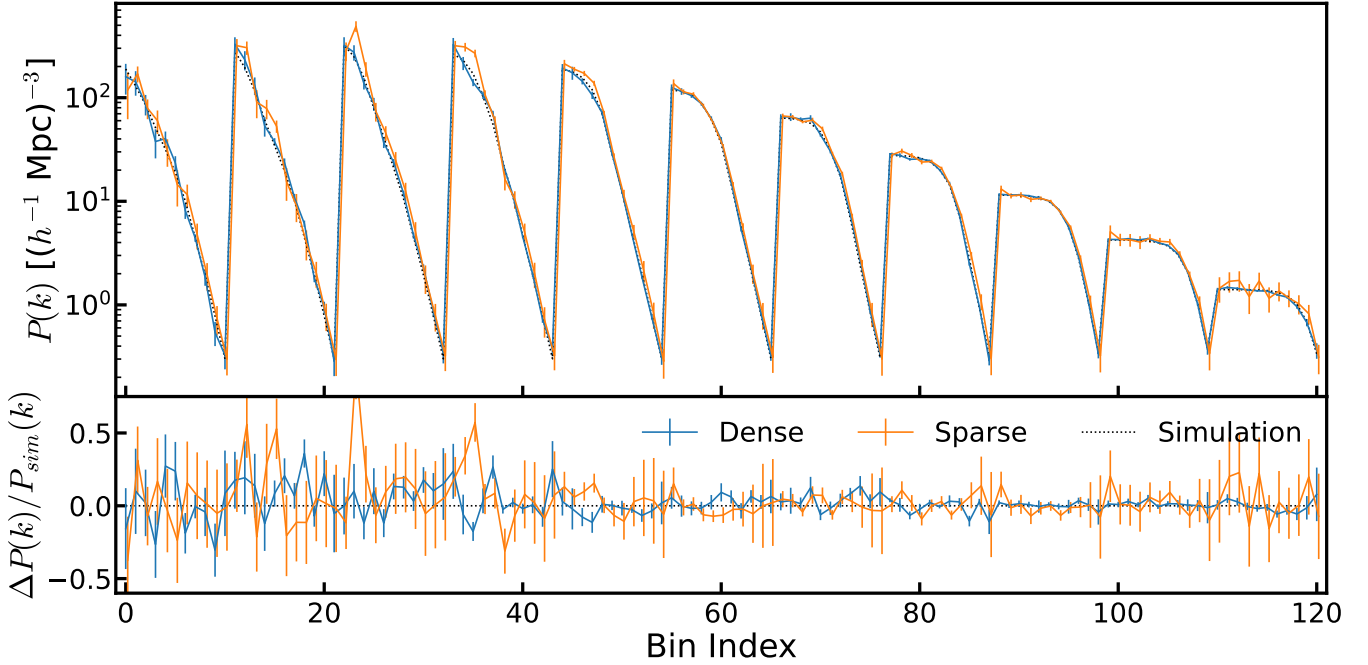


Figure 2. Reconstructed band-powers and associated errors from the dense and sparse mock catalogs shown as a function of bin index. Bins are ordered by k_{\perp} first, and then by k_{\parallel} . The bottom panel shows the relative residuals with respect to the theory input power spectrum. We find good agreement across a range of scales with reasonable error estimates.

sample we assume a signal-to-noise distribution similar to that found in the CLAMATO survey (Lee et al. 2018; Horowitz et al. 2022a). We assume the S/N is drawn from a power-law distribution with minimum value $S/N_{\min} = 1.0$ (i.e. $dn_{\text{los}}/d(S/N) \propto S/N^{\alpha}$) with spectral amplitude $\alpha = 2.7$. We also assume a maximal amplitude $S/N_{\max} = 10.0$ due to detector saturation on the bright end. We emphasize that we are not providing forecasts for both surveys but emulate Ly- α -specific survey geometries and number densities.

We choose a highly anisotropic angular selection function to mimic irregularities in survey structure, including bright star masks, unobserved stripes, and deep fields. We pad the edges by $10 h^{-1}$ Mpc to avoid edge-effects due to the periodic nature of the Fourier operations used in our reconstruction. Note that we choose the same geometry for the dense and sparse fields, shown in Fig. 1. Additionally, we assume that background sources are uniformly distributed radially in the volume, resulting in a linear redshift distribution of data pixels. To increase the level of realism, we include Damped Lyman Alpha systems (DLAs) where the flux is damped in a region of 15 angstroms (with no explicit modelling of their damping wings or other features).⁷ Each sight-line has a 10% chance of having a DLA. For each DLA region, we mask out the DLA in noise, i.e. we increase the noise in those regions to very large values. This effectively removes them from the likelihood analysis.

5 RESULTS

In this section, we present the results of our band-power and covariance estimator on GRFs with a fiducial Kaiser power spectrum with a non-linear correction term obtained from hydrodynamical simulations (McDonald 2003). We use the approach described in Section 2,

⁷ Note that we make the simplifying assumption that DLAs are uncorrelated with the underlying structure.

starting from band-powers normally distributed around their true values, with a standard deviation of 0.3 times the fiducial power spectra, $P_{\text{F}}(k, \mu)$. For each optimization step, we average over 40 simulations with a convergence criteria of $\theta_{\text{tol}} = 10^{-5}$. This takes about 2 hours (approximately 2000 steps) on a 1 GPU (NVIDIA A100-SXM 40Gb) core including the Hessian estimation.

We show the band-power results of our reconstruction in Fig. 2 with errors from the reconstructed covariance matrix using Eq. 6. To generate an intuitive understanding for the reader, we also show the projection into $\{k, \mu\}$ space in Fig. 3 for both configurations. In both, reconstructed space and projected space, we find reasonable error estimates which generally follow a Gaussian distribution. In our reconstructed space, we find a reduced chi-squared, χ^2 , of 1.31 and 1.11 for the dense and sparse configurations, respectively.

The corresponding correlation matrix is shown in Fig. 4. This matrix is averaged over 20 realizations to reduce numerical noise. The correlation matrix is defined as

$$\mathbf{R}^{ij} \equiv \frac{\Sigma_{ij}}{\sqrt{\Sigma_{ii}\Sigma_{jj}}}, \quad (12)$$

and by construction it is unity along the diagonal. The covariance matrix is denoted by Σ of power spectra in bins i, j . We find relatively small off-diagonal contributions which arise from the complex survey geometry. As expected, these contributions have higher amplitude in the dense survey as the data is more informative. The particularities of the survey geometry impact the specific μ dependencies in the error-bars and may not be generic for all surveys.

6 CONCLUSIONS & OUTLOOK

In this work, we have presented MAPLE, a Wiener-filter-based optimization Ly- α three-dimensional power spectrum and full covariance/window function for two realistic survey configurations. This

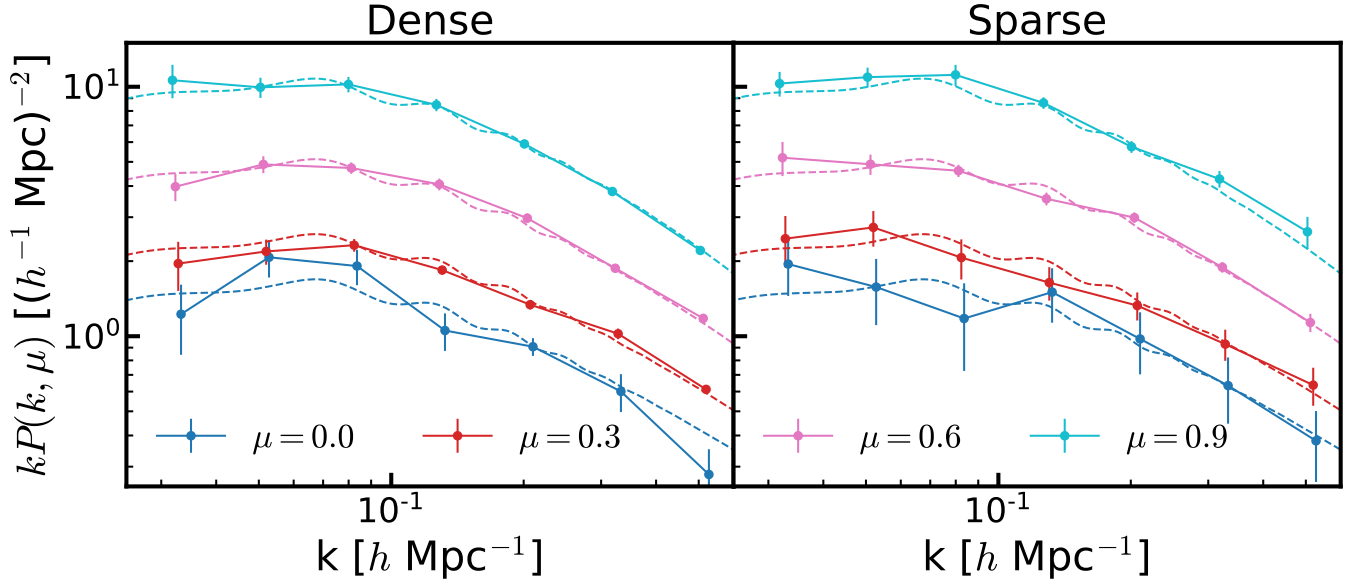


Figure 3. Projection of the reconstructed power spectrum and covariance from $\{k_{\perp}, k_{\parallel}\}$ space to $\{k, \mu\}$ space. The error bars are taken from the diagonal of the square root of the covariance matrix in $\{k_{\perp}, k_{\parallel}\}$ space and also projected. We perform this projection by interpolating in $\{k_{\perp}, k_{\parallel}\}$ space and then outputting values along lines of constant μ . The left (right) panel shows results from the dense (sparse) mock catalog. There is good agreement between the underlying model and our reconstruction.

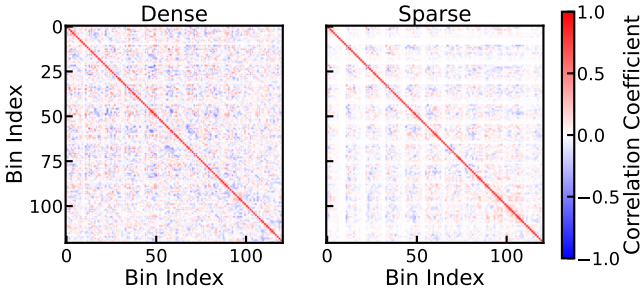


Figure 4. Correlation matrix of the reconstructed band-powers from the dense and sparse catalogs for the particular geometry shown in Fig. 1. Lack of off-diagonal correlations present in certain band-powers in the sparse catalog indicates lack of constraining power in that bin due to survey properties, i.e. the prior dominates the resulting likelihood. The grid structure is to be expected as the bins are ordered by k_{\perp} and then by k_{\parallel} (see Figure 2).

method is fast and scalable, and we make it publicly available on GitHub. With this method we find a consistent reconstructed result with good reduced χ^2 error properties.

In this work, we choose to optimize each individual band-power on a rectangular grid, as it is the basis of the transfer function. This choice allows greatest flexibility and independence, as it can be used to constrain any P3D model. However, depending on the analysis of interest this might not be optimal. Also, one can directly use any differentiable parameterized model of $k_{\perp} - k_{\parallel}$ to directly infer model parameters from Ly- α Forest data. This could include directly using Eq. (9) (if given a differentiable model for $P_{\perp}(k)$ with respect to cosmological parameters), using an emulator for the whole P3D distribution, analytical P3D models (Ivanov 2024), interpolation over multipoles, etc.

The main goal of this letter is to demonstrate a promising new approach to measuring the P3D for Ly- α forest data. While our analysis choices are idealized and need to be tested on realistic mocks prior to application on Ly- α data, we have shown that the method is

fast, scalable, and can be used to estimate the P3D and its covariance. While beyond the scope of this work, the underlying framework is flexible and allows joint modelling/marginalization over survey systematics. For example, one can jointly optimize the band-powers with QSO continuum estimation (e.g. PCA components, i.e. Lee et al. (2012)) or DLA identification allowing for consistent propagation of uncertainties throughout the data analysis pipeline-line into the final cosmological analysis. This is particularly important for modes along the line of sight, which have significant correlated error contributions.

An alternative approach to cosmological inference from Ly- α forest data would be a dynamical reconstruction approach where the initial matter density phases are reconstructed as opposed to the late time flux field (Horowitz et al. 2019a, 2021). While these approaches have been used successfully for large-scale structure inference (Horowitz et al. 2022a), applying the techniques in this paper to cosmological inference would be difficult due to the complex hydrodynamical modelling. In particular, uncertainty in the hydrodynamics must be accounted for in a differentiable way in order for the underlying optimization to be computationally tractable. This could be done via parameterized models (Kooistra et al. 2022) or latent space deep learning surrogate modelling (Horowitz et al. 2022b). We leave this full analysis to future work.

ACKNOWLEDGEMENTS

We thank Pat McDonald, Andreu Font-Ribera, Julien Guy, Nathalie Palanque-Delabrouille, Uroš Seljak, and Marius Millea for their helpful insights.

This work was partially supported by the DOE’s Office of Advanced Scientific Computing Research and Office of High Energy Physics through the Scientific Discovery through Advanced Computing (SciDAC) program. This research used resources of the National Energy Research Scientific Computing Center, a DOE Office of Science User Facility supported by the Office of Science of the U.S. Department of Energy under Contract No. DEC02-05CH11231.

DATA AVAILABILITY

The data underlying this article will be shared on reasonable request. We make our code implementation publicly available⁸.

REFERENCES

- Alsing J., Wandelt B., 2018, *MNRAS*, 476, L60
- Arinyo-i-Prats A., Miralda-Escudé J., Viel M., Cen R., 2015, *J. Cosmology Astropart. Phys.*, 2015, 017
- Busca N. G., et al., 2013, *A&A*, 552, A96
- Cauci S., Colombi S., Pichon C., Rollinde E., Petitjean P., Sousbie T., 2008, *MNRAS*, 386, 211
- Chabanier S., et al., 2019, *J. Cosmology Astropart. Phys.*, 2019, 017
- Croft R. A. C., Weinberg D. H., Pettini M., Hernquist L., Katz N., 1999, *ApJ*, 520, 1
- Croft R. A. C., Weinberg D. H., Bolte M., Burles S., Hernquist L., Katz N., Kirkman D., Tytler D., 2002, *ApJ*, 581, 20
- Cuceu A., Font-Ribera A., Joachimi B., Nadathur S., 2021, *MNRAS*, 506, 5439
- Cuceu A., Font-Ribera A., Nadathur S., Joachimi B., Martini P., 2023, *Phys. Rev. Lett.*, 130, 191003
- DESI Collaboration et al., 2016, arXiv e-prints, p. arXiv:1611.00036
- Font-Ribera A., McDonald P., Slosar A., 2018, *J. Cosmology Astropart. Phys.*, 2018, 003
- Garny M., Konstandin T., Sagunski L., Tulin S., 2018, *J. Cosmology Astropart. Phys.*, 2018, 011
- Goldstein S., Hill J. C., Iršič V., Sherwin B. D., 2023, *Phys. Rev. Lett.*, 131, 201001
- Gordon C., et al., 2023, arXiv e-prints, p. arXiv:2308.10950
- Greene J., Bezanson R., Ouchi M., Silverman J., the PFS Galaxy Evolution Working Group 2022, arXiv e-prints, p. arXiv:2206.14908
- Gunn J. E., Peterson B. A., 1965, *Astrophysical Journal*, vol. 142, p. 1633-1636, 142, 1633
- Horowitz B., Lee K.-G., White M., Krolewski A., Ata M., 2019a, *ApJ*, 887, 61
- Horowitz B., Seljak U., Aslanyan G., 2019b, *J. Cosmology Astropart. Phys.*, 2019, 035
- Horowitz B., Zhang B., Lee K.-G., Kooistra R., 2021, *ApJ*, 906, 110
- Horowitz B., et al., 2022a, *ApJS*, 263, 27
- Horowitz B., Dornfest M., Lukić Z., Harrington P., 2022b, *ApJ*, 941, 42
- Iršič V., et al., 2017, *Phys. Rev. D*, 96, 023522
- Iršič V., et al., 2024, *Phys. Rev. D*, 109, 043511
- Ivanov M. M., 2023, arXiv e-prints, p. arXiv:2309.10133
- Ivanov M. M., 2024, *Phys. Rev. D*, 109, 023507
- Kaiser N., 1987, *MNRAS*, 227, 1
- Karacaylı N. G., et al., 2022, *MNRAS*, 509, 2842
- Karacaylı N. G., Font-Ribera A., Padmanabhan N., 2020, *MNRAS*, 497, 4742
- Karim M. L. A., Armengaud E., Mention G., Chabanier S., Ravoux C., Lukić Z., 2023, Measurement of the small-scale 3D Lyman- α forest power spectrum (arXiv:2310.09116)
- Kim T. S., Viel M., Haehnelt M. G., Carswell R. F., Cristiani S., 2004, *MNRAS*, 347, 355
- Kooistra R., Lee K.-G., Horowitz B., 2022, *ApJ*, 938, 123
- Kraljic K., et al., 2022, *MNRAS*, 514, 1359
- Laux S., 1995, in *Simulation of Semiconductor Devices and Processes: Vol. 6*, pp 404–407
- Lee K.-G., Suzuki N., Spergel D. N., 2012, *AJ*, 143, 51
- Lee K.-G., et al., 2018, *ApJS*, 237, 31
- Li Y., et al., 2022, arXiv e-prints, p. arXiv:2211.09958
- McDonald P., 2003, *ApJ*, 585, 34
- McDonald P., Eisenstein D. J., 2007, *Phys. Rev. D*, 76, 063009
- McDonald P., et al., 2005, *ApJ*, 635, 761
- Millea M., 2022, arXiv e-prints, p. arXiv:2209.10512
- Millea M., Seljak U., 2022, *Phys. Rev. D*, 105, 103531
- Newman A. B., et al., 2020, *ApJ*, 891, 147
- Palanque-Delabrouille N., et al., 2013, *A&A*, 559, A85
- Pedersen C., Font-Ribera A., Rogers K. K., McDonald P., Peiris H. V., Pontzen A., Slosar A., 2021, *JCAP*, 05, 033
- Peebles P. J. E., Yu J. T., 1970, *ApJ*, 162, 815
- Ravoux C., et al., 2023, *MNRAS*, 526, 5118
- Scheuer P., 1965, *Nature*, 207, 963
- Seljak U., Aslanyan G., Feng Y., Modi C., 2017, *J. Cosmology Astropart. Phys.*, 2017, 009
- Seo H.-J., Eisenstein D. J., 2003, *ApJ*, 598, 720
- Slosar A., et al., 2011, *J. Cosmology Astropart. Phys.*, 2011, 001
- Slosar A., et al., 2013a, *J. Cosmology Astropart. Phys.*, 2013, 026
- Slosar A., et al., 2013b, *J. Cosmology Astropart. Phys.*, 2013, 026
- Sunyaev R. A., Zeldovich Y. B., 1970, *Ap&SS*, 7, 3
- Viel M., Becker G. D., Bolton J. S., Haehnelt M. G., 2013, *Phys. Rev. D*, 88, 043502
- Villasenor B., Robertson B., Madau P., Schneider E., 2023, *Phys. Rev. D*, 108, 023502
- Yèche C., Palanque-Delabrouille N., Baur J., du Mas des Bourboux H., 2017, *J. Cosmology Astropart. Phys.*, 2017, 047
- de Belsunce R., Philcox O. H. E., Irsic V., McDonald P., Guy J., Palanque-Delabrouille N., 2024, arXiv e-prints, p. arXiv:2403.08241
- du Mas des Bourboux H., et al., 2020, *ApJ*, 901, 153

This paper has been typeset from a $\text{\TeX}/\text{\LaTeX}$ file prepared by the author.

⁸ <https://github.com/bhorowitz/MAPLE>